

Orientational disorder in 1,2,3-trichloro-4,5,6-trimethylbenzene. A single crystal deuterium NMR study of the site populations and dynamics

Thomas Bräuniger,^a Raphy Poupko,^a Zeev Luz,^{*a} Detlef Reichert,^b Herbert Zimmermann,^c Heike Schmitt^c and Ulrich Haeberlen^c

^a Weizmann Institute of Science, Rehovot 76100, Israel

^b Fachbereich Physik, Martin-Luther-Universität Halle-Wittenberg, 06108 Halle, Germany

^c A.G. Molekülkristalle, Max-Planck-Institut für Medizinische Forschung, Jahnstrasse 29, 69120 Heidelberg, Germany

Received 8th November 2000, Accepted 27th February 2001

First published as an Advance Article on the web 11th April 2001

Deuterium NMR measurements on powder and single crystal samples of 1,2,3-trichloro-4,5,6-trimethylbenzene (TCTMB) specifically deuterated at the central methyl group (TCTMB-d₃) are reported. The compound exhibits three solid phases: (I) A high temperature phase, just below the melting point (400 to 499 K), of unknown structure. (II) An intermediate monoclinic phase (268 to 400 K). (III) A low temperature triclinic phase (<268 K). Earlier X-ray investigations of the latter two phases indicate that they are, respectively, well ordered (Phase III at 173 K), and orientationally disordered, with the TCTMB molecules statistically aligned along the six possible orientations of the benzene core (Phase II at 298 K). In contrast to these observations the deuterium NMR results show a continuous growth, with temperature, of orientational disorder already in Phase III. The transition to Phase II involves a discontinuous increase in the disorder, but a considerable degree of order is retained in this phase even at high temperatures. This ordering reflects the non-equal population distribution of the molecular orientation in the crystal lattice sites. A quantitative analysis of the deuterium NMR spectra provided detailed information on this distribution and its temperature dependence in the solid phases of TCTMB. The deuterium NMR spectra also exhibit characteristic dynamic effects. As a function of increasing temperature, four dynamic regions can be distinguished: (i) Below 15 K, the spectrum exhibits features typical of coherent quantum-mechanical tunneling of the CD₃ groups. (ii) Above 15 K, up to about 170 K, there is fast classical (incoherent) reorientation of the methyl groups, but otherwise a rigid molecular lattice. (iii) Between 180 and 250 K, the spectra exhibit dynamic lineshape changes reflecting the onset of six-fold jumps of the TCTMB molecules. (iv) Above 250 K the spectra correspond to a dynamically averaged, but temperature dependent, quadrupolar splitting, reflecting the changes in the orientational distribution of the TCTMB molecules. This region includes the phase transitions, III to II and II to I. *T*₁ relaxation measurements over the entire temperature range yielded kinetic parameters for the molecular six-fold jumps (*k*(260 K) = 7 × 10⁶ s⁻¹, Δ*E* = 38.5 kJ mol⁻¹), as well as for the incoherent methyl group reorientation (*k*(25 K) = 1 × 10⁹ s⁻¹, Δ*E* = 2.8 kJ mol⁻¹).

1 Introduction

It is well known that mixed hexasubstituted benzenes of the general formula C₆Cl_{*n*}(CH₃)_{6-*n*} exhibit orientational disorder in the solid state. This is a consequence of the fact that the van der Waals radii of the chlorine and methyl groups are quite similar, so that they can be interchanged without severely affecting the packing energy of the crystalline lattice. Extensive dielectric measurements were carried out on a variety of chloro-methylbenzenes as early as 1940 by White *et al.*,¹ which indicated that the disorder in these compounds is dynamic, involving planar molecular reorientation. These early findings were confirmed by subsequent studies, using X-ray diffractometry, proton *T*₁ and wide line NMR spectroscopy and calorimetry. A brief review summarizing the current knowledge on the dynamic disorder in halogenomethylbenzenes can be found in a recent paper by Tazi *et al.*²

In this paper we present a deuterium NMR study of the orientational disorder in 1,2,3-trichloro-4,5,6-trimethylbenzene (TCTMB). For the measurements we used powder and single crystal samples of TCTMB, specifically deuterated at the

central methyl group, C₆Cl₃(CH₃)(CD₃)(CH₃) (TCTMB-d₃). It was shown earlier³ by differential scanning calorimetry (DSC) that TCTMB exhibits three solid phases, with transition temperatures, 500 (melting), (401 ± 3) and (260 ± 3) K. The corresponding transitions for our TCTMB-d₃ sample are shown in the DSC thermogram in Fig. 1. They are essentially the same as those of the isotopically normal compound. We will refer to the three solid phases, in order of decreasing temperature, as Phase I (400 to 499 K), Phase II (268 to 400 K) and Phase III (<268 K), respectively. No studies on Phase I have been published so far. The X-ray structures of Phases II and III were investigated by Fourme and coworkers, at, respectively, 298⁴ and 173 K.⁵ Phase II was found to be monoclinic and orientationally disordered, while Phase III is triclinic and essentially ordered. The crystal structures of these phases are very relevant for the interpretation of the present NMR results and we therefore describe them in some detail in a separate section (Section 2) below.

Already before the crystal structures of TCTMB were determined it was realized, on the basis of dielectric measurements, that the molecules in the solid phases of this compound

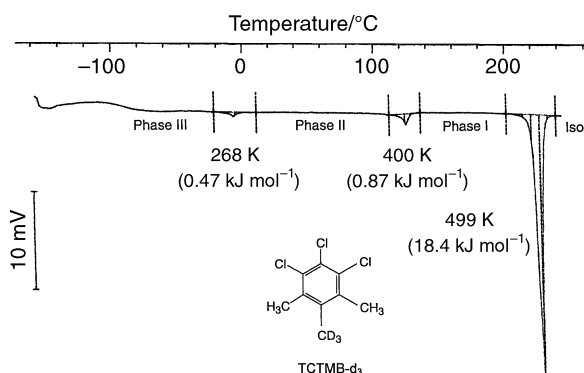


Fig. 1 DSC thermogram of the specifically deuterated TCTMB sample (TCTMB- d_3). 9.6 mg of the material were used, with a heating rate of 10 K min^{-1} . The vertical dashed bars indicate the integration range for computing the phase transition enthalpies.

undergo fast planar reorientation,¹ implying the presence of a degree of disorder even in the low-temperature Phase III. These findings were later confirmed and further investigated by additional dielectric relaxation studies,³ as well as wide line proton NMR⁶ and relaxation measurements.⁷ Although these studies resulted in numerical estimates for the kinetic parameters of the molecular motions, neither the dielectric nor the earlier NMR measurements could provide detailed information on the nature of the disorder (population distribution) and its dynamics at the molecular level. In the present work we apply the method of single crystal deuterium NMR to investigate the disorder in the solid phases II and III of TCTMB. As will be seen, this method is ideal for such studies. We show that the “disordered” Phase II is, in fact, partially ordered, in the sense that the various molecular directions are not equally populated and we determine the population distribution as a function of the temperature. Likewise, Phase III, which is well ordered at low temperatures, becomes gradually disordered on heating and we provide quantitative estimates for this disorder. The dynamics of the disorder in both phases corresponds to 60° jumps between the minima of the pseudo-six-fold-symmetric potential in which the TCTMB molecules are embedded. Analysis of the NMR results provides estimates for the kinetic parameters of this process. Finally, we also determined kinetic parameters for the three-fold incoherent jumps of the methyl groups, at low temperatures, and show that, below 15 K, this thermally activated process is taken over by coherent quantum mechanical tunneling.

2 The crystal structure of Phases II and III

The X-ray structure of Phase II was determined by Fourme *et al.*⁴ at 298 K. It was found to be monoclinic, belonging to the space group $P2_1/c$ with two symmetry related molecules, M and M', per unit cell. The dimensions of this unit cell are: $a_m = 8.22 \text{ \AA}$, $b_m = 3.88 \text{ \AA}$, $c_m = 17.16 \text{ \AA}$, with $\beta_m = 119.33^\circ$. Projections of this unit cell down the a_m^* and b_m axes are shown in Fig. 2(a) and (b), respectively. Since in this space group four asymmetric units are expected per unit cell, it follows that the molecules must occupy sites of inversion symmetry. However, as the TCTMB molecules lack such a symmetry, it must be assumed that they are orientationally disordered such that on the average the lattice sites are centrosymmetric. The molecular planes were found to lie nearly parallel to the $a_m c_m$ crystal planes, with their normals subtending an angle of 21.8° with the b_m axis. The average inversion symmetry implies that if we associate with each TCTMB molecule an arrow pointing from the center chlorine atom to the center methyl group (CD_3 in TCTMB- d_3), these arrows will be statistically pointing “up” and “down” throughout the lattice. We refer to this type of disorder as

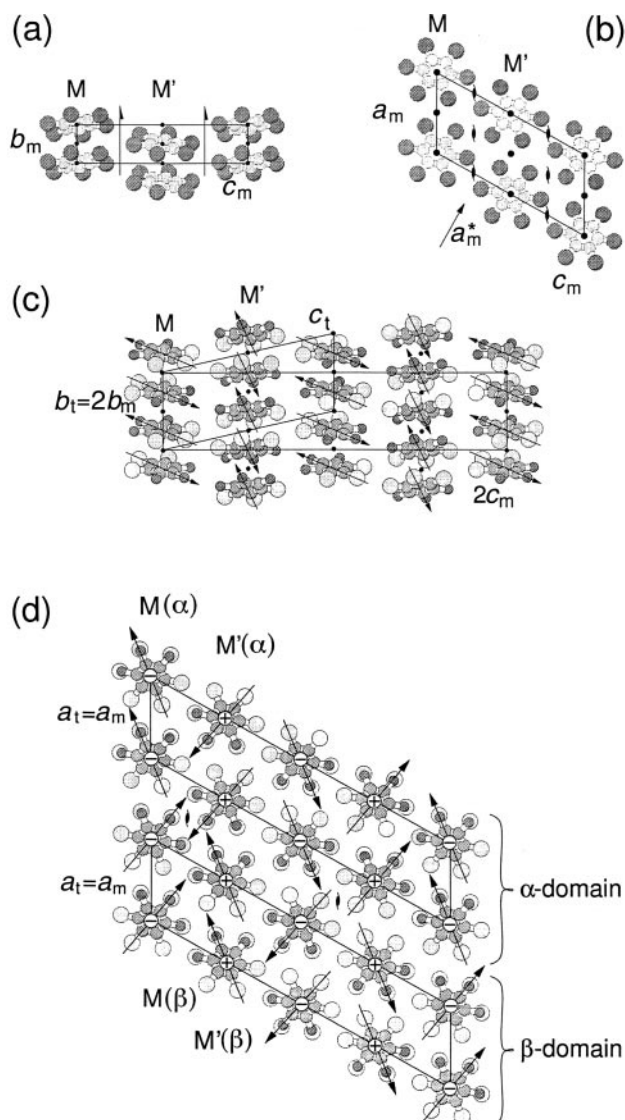


Fig. 2 Projections of the crystal structures of TCTMB in the monoclinic phase II and triclinic phase III, based on X-ray diffraction data recorded at 298⁴ and 173 K,⁵ respectively. In the Phase II, all substituents of the benzene rings are indicated by identical dark-dotted spheres. In the Phase III, the methyl groups are indicated by small, dark-dotted spheres, the chlorines by large, light-dotted spheres. (a), (b) Projections of Phase II unit cell down the crystallographic a_m and b_m axes, respectively. M and M' are monoclinically related molecules. (c) Projection of the Phase III unit cell down the a_t^* axis. b_t and c_t are the axes of the primitive unit cell, $b_t^* = b_t = 2b_m$ and $c_t^* = 2c_m$ are axes of the (non-primitive) triclinic supercell. The arrows indicate the direction of polarization of the molecules. The molecules M and M' are not symmetry related. (d) Two projections down the b_t^* axis of the triclinic supercell. The two projections correspond to the α and β forms of the top layer in each domain. The two domains are related by two-fold screw axes as shown. The + and - symbols at the center of the molecules indicate relative displacements along b_t^* . The molecules M and M' in the same domain are not symmetry related, but the pairs M(α), M'(β) and M(β), M'(α) are pairwise related by twofold screw axes.

“polar disorder”.⁸ Moreover, the X-ray results⁴ also indicate that these arrows are equally distributed along the six directions of the pseudo-hexagonally-symmetric TCTMB molecule, corresponding to complete planar disorder. Below we will demonstrate that this is actually not the case.

The X-ray structure of Phase III was determined by Fourme and Renaud⁵ at 173 K. They found this phase to be triclinic, belonging to the space group $P\bar{1}$. The transition from the monoclinic Phase II to this phase involves almost no

change in the position of the molecules or in the orientation of their planes (*i.e.*, the directions of the normals to the molecular planes remain essentially the same as in the monoclinic phase). Rather, the transition involves, predominantly, the setting-in of orientational order: At the temperature at which the X-ray measurements were performed, the directions of the arrows associated with each molecule are fixed and each lattice site has a well defined polarization (preferred directions of the arrows). A projection of the triclinic unit cell down the a_t^* axis is shown in Fig. 2(c). It can be patterned on the monoclinic Phase II lattice by shifting the origin by $\frac{1}{2}b_m$ along b_m and setting $a_t = a_m$, $b_t = 2b_m$, $c_t = \sqrt{b_m^2 + c_m^2}$, with $\alpha_t = \arctan(c_m/b_m)$, $\beta_t = \arccos[(c_t/c_m)(a_t/a_m)]$, $\gamma_t = \pi/2$. This unit cell has twice the volume of the monoclinic unit cell, with four molecules; two of type M, related by an inversion center, and two of type M', also related by inversion. The two types of molecules are, however, not symmetry related anymore, as they are now polarized in different orientations.

For certain purposes it is convenient to define a triclinic supercell with lattice dimensions, $a_t^s = a_m$, $b_t^s = 2b_m$, $c_t^s = 2c_m$ and $\alpha_t^s = \gamma_t^s = \pi/2$, $\beta_t^s = \beta_m$. A projection of this cell down the a_t^{s*} axis is also shown in Fig. 2(c). This non-primitive cell has twice the volume of the triclinic primitive cell (four times the volume of the monoclinic unit cell) and contains eight molecules. It has, however, the advantage of having two right angles and, as discussed by Fourme and Renaud,⁵ allows treatment of this phase within the simpler framework of monoclinic symmetry. The parameters of this supercell at 173 K are: $a_t^s = 8.12 \text{ \AA}$, $b_t^s = 7.62 \text{ \AA}$, $c_t^s = 34.25 \text{ \AA}$, with $\beta_t^s = 119.33^\circ$. These dimensions are somewhat smaller than expected from the relations given above and from the values determined for the monoclinic Phase II at 298 K. The difference is ascribed to thermal contraction.

Another projection of the triclinic supercell, now down the b_t^s axis is shown in the upper diagram of Fig. 2(d) (labeled " α -domain"). As pointed out by Fourme and Renaud,⁵ the $P\bar{1}$ unit cell can appear in two lattice forms related to each other by a two-fold screw axis parallel to b_t . The two forms are referred to as α and β and a projection of the corresponding β form is also shown in Fig. 2(d). In principle crystals can crystallize as pure α or pure β forms, but in reality mixed crystals are usually obtained, with a statistical distribution of the two forms.⁹ On a mesoscopic level these crystals consist of a mosaic of α and β domains separated by domain walls where the molecular polarization switches from that of one form to the other. Inspection of Fig. 2(c) and (d) shows that such a mixed crystal contains two sets of symmetry non-related molecules. One set consists of the M molecules in the α domains, M(α) and the M' molecules in the β domains, M'(β). The other set consists of the M'(α) and M(β) molecules. Within each set the primed and unprimed molecules are related by twofold screw axes. (Note, however, that the translation part of the screw operation which transforms α into β is different from that which transforms β into α . Therefore, by combining cells

from the α and β domains, it is not possible to construct a genuine monoclinic supercell.) In each domain, adjacent M (M') molecules in the stack along the b axis are related by inversion centers. Since molecules related by inversion are magnetically equivalent, we expect in a single crystal $^2\text{H-NMR}$ spectrum, for a general direction of the magnetic field, signals from four types of molecules, which are pairwise related by monoclinic symmetry. Accordingly, we shall analyze the NMR results of Phase III in the framework of monoclinic symmetry. We must keep in mind, however, that this pseudosymmetry is based on the assumption of a statistical distribution of α and β domains in the crystal. As we shall see this is not always so.

For later reference we summarize in Table 1 relevant X-ray data on the molecular orientations in Phases II⁴ and III.⁵ These data (unit vectors along molecular bond directions) are given in the standard orthogonal system (SOS), abc^* , which is common to the monoclinic cell and triclinic supercell.

3 Experimental

3.1 Material and crystal growth

Two deuterated isotopologues of TCTMB were prepared, *viz.*, TCTMB perdeuterated in the three methyl groups (TCTMB- d_9) and TCTMB specifically deuterated in the center methyl group (TCTMB- d_3). They were obtained by chlorination of the corresponding deuterated trimethylbenzenes (TMB- d_{12} and TMB- d_3). In a typical experiment 20 g of distilled TMB were dissolved in 220 ml petrol ether (bp = 60–95 °C) and 200 mg of iodine were added. A slow stream of chlorine gas was passed through the solution for about 2 h, resulting in decoloration and warming of the reaction mixture. The mixture was then allowed to cool and kept in ice overnight, yielding after filtration, a first crop of 3 g TCTMB. The filtrate was then subjected to a second chlorination until no further heating of the reaction mixture was detected. Cooling as above and filtering yielded another crop of 6 g TCTMB. The combined harvest was recrystallized twice from ethanol (with a few drops of chloroform added), yielding 6 g of white TCTMB crystalline needles.

TMB- d_{12} was prepared from the isotopically normal compound by catalytic exchange with D_2O , using 10% Pt/C. The mixture was kept in a stainless steel pressure vessel at 300 °C for one week. The deuterated TMB was isolated and the procedure repeated two more times using fresh D_2O and Pt/C. After distillation, 90% of the TMB was recovered as TMB- d_{12} , with 96–98% deuterium enrichment at the methyl groups, as determined by NMR and mass spectrometry.

Trimethylbenzene specifically deuterated in the center methyl group, $\text{C}_6\text{H}_3(\text{CH}_3)(\text{CD}_3)(\text{CH}_3)$ (TMB- d_3) was prepared by a three-step synthesis from 2,6-dimethylbenzoic acid (DMBA), involving reduction to deuterated 2,6-dimethylbenzylalcohol- d_2 , bromination to the corresponding

Table 1 Polar angles, θ , ϕ , (in degrees) of the substituent bond directions, 1, 2 and 3, and of the normal to the molecular plane, \perp , for the M and M' molecules in the Phases II (at 298 K⁴) and III (at 173 K⁵) of TCTMB as obtained from X-ray diffraction (see Fig. 2). The angles refer to the abc^* SOS. The molecules in the upper part of the Table are related to the corresponding ones in the lower part, by monoclinic symmetry, *i.e.* by a 180° rotation about b ($\theta \rightarrow \pi - \theta$, $\phi \rightarrow \pi - \phi$)

Mol.	Phase	Subst. 1	Subst. 2	Subst. 3	\perp
M	II	111.5, 340.9	51.8, 335.0	170.3, 9.4	85.0, 68.8
M(α)	III	110.4, 341.1 ^a	50.9, 333.8	168.8, 11.6	83.9, 68.8
M(β)	III	110.9, 342.1	51.3, 334.2 ^a	168.9, 15.9	83.3, 69.6
M'	II	68.5, 199.1	128.2, 205.0	9.7, 170.6	95.0, 111.2
M'(β)	III	69.6, 198.9 ^a	129.1, 206.2	11.2, 168.4	96.1, 111.2
M'(α)	III	69.1, 197.9	128.7, 205.8 ^a	11.1, 164.1	96.7, 110.4

^a Polarization direction of the molecule at low temperatures.

Table 2 Effective orientations of the goniometer axis, θ , ϕ , in the abc^* SOS used in the analysis of the twinned Crystal A

Molecule	Major twin	Minor twin ^b
M	103.0, 285.5	77.0, 74.5
M' ^a	77.0, 254.5	103.0, 105.5

^a Effective orientation of the goniometer axis for the M' molecule, obtained from the corresponding entries for M by 180° rotation about the crystallographic b axis ($\theta \rightarrow \pi - \theta$, $\phi \rightarrow \pi - \phi$). ^b Effective orientation of the goniometer axis for the minor twin, obtained from the corresponding entries for the major twin, by 180° rotation about the crystallographic a axis ($\theta \rightarrow \pi - \theta$, $\phi \rightarrow 2\pi - \phi$).

benzyl bromide and finally debromination. A solution of 50 g DMBA in dry ether was added to 20 g LiAlD₄ in ether and the mixture refluxed for several hours. The mixture was then hydrolyzed, first with D₂O, then with H₂SO₄ and subsequently extracted with ether. After evaporation of the solvent and distillation of the residue, 37 g of 2,6-dimethylbenzylalcohol-d₂ were recovered. The sample was redissolved in ether, and 27 g of PBr₃ were slowly added. The mixture was stirred for several hours at room temperature and then refluxed overnight. After cooling the mixture was poured onto ice and three times extracted with ether. The solution was then washed with H₂O and dried over Na₂SO₄. After evaporating the solvent, 52 g of 2,6-dimethylbenzylbromide-d₂ were recovered. In the final step of the synthesis the latter product was added to a solution containing 18 g LiAlD₄ in ether and the mixture refluxed for 8 h. After work up, 28 g of the desired TMB-d₃ were obtained. From NMR and mass spectrometry, the deuteration level of this product was found to be 98%.

Single crystals of TCTMB were grown in vacuum sealed tubes, using a Bridgeman–Stockberger crystal-growing furnace.

3.2 NMR measurements and goniometry

The deuterium NMR measurements were performed on two spectrometers: (i) The Heidelberg home-built spectrometer, operating at a deuterium frequency of 72 MHz, using a single pulse detection ($\pi/2$ pulse width, 3.0 μ s). It was predominantly used for sub 100 K measurements. (ii) A Bruker CXP300 spectrometer, controlled by a Tecmag pulse programmer, with a deuterium frequency of 46.1 MHz and using quadrupole echo detection ($\pi/2$ pulse width 2.5 μ s, echo delay 15 μ s). Both spectrometers were equipped with a goniometer probe, allowing rotation of the crystal about an axis perpendicular to the magnetic field. The deuterium 2D exchange spectrum was acquired on a Varian Inova 400 (deuterium frequency, 61.4 MHz).

The melt-grown crystals were cleaved and cut to suitable size ($\sim 4 \times 4 \times 8$ mm³), and then fixed on PVC rods using epoxy glue. The orientations of the goniometer rod in the crystal SOS were determined by optical goniometry and subsequently fine-tuned by fitting the NMR rotation spectra. For protection, the crystals were housed in standard thin-walled 5 mm glass tubes. The single crystal measurements were made on two specimens, labeled A and B. Most measurements were performed on Crystal A, which happened to be twinned with a major and a minor component. The two components shared the crystallographic a axes, but had antiparallel b axes. This crystal had the goniometer rod glued at a general orientation in its SOS. The polar angles of the goniometer in this crystal are summarized in Table 2. The second crystal, B (not twinned), was used for relaxation measurements at low temperatures and for acquiring spectra in the tunneling regime. It had the goniometer rod glued parallel to its b axis.

4 Results and discussion

4.1 Deuterium NMR spectra of a powder sample

As a preliminary study of the TCTMB system we first recorded the deuterium NMR spectra of a powder sample of TCTMB-d₃ over a wide temperature range, covering all three solid phases. Examples of such spectra are shown in Fig. 3. In the low temperature range of Phase III, below 130 K, the spectrum is characteristic of a rigid powder due to a nearly axially symmetric quadrupolar tensor, $\eta = 0.07$, $|v_Q^{(CD_3)}| = 38.5$ kHz, where $v_Q^{(CD_3)} = \frac{3}{4}Q_{ZZ}^{(CD_3)}$ is the major quadrupolar splitting and $Q_{ZZ}^{(CD_3)}$ is the major principal component of the quadrupole coupling tensor, defined in the usual manner, $Q_{ZZ}^{(CD_3)} = e^2q^{(CD_3)}Q/h$. The low temperature spectrum in Fig. 3 is consistent with rapidly reorienting methyl groups, but otherwise static TCTMB molecules. For this situation $v_Q^{(CD_3)}$ is expected to be $\frac{1}{2}\langle 3\cos^2\tau - 1 \rangle v_Q^{CD} = -\frac{1}{3}v_Q^{CD} \approx -40$ kHz, where v_Q^{CD} is the major quadrupole splitting of an aliphatic deuteron (~ 120 kHz) and τ is the angle between the C–D bond direction and the C_3 symmetry axis of the CD₃ group, which we assumed to be tetrahedral. Hence, for TCTMB-d₃ at 130 K, $v_Q^{(CD_3)} = \frac{3}{4}Q_{ZZ}^{(CD_3)} = -38.5$ kHz, where the angular brackets in the superscript indicate averaging over the methyl group rotation, and Z is parallel to the C–CD₃ bond direction.

Between 130 and about 260 K, the spectrum broadens and eventually coalesces to a much narrower powder pattern, with an average quadrupole splitting of $|\langle v_Q \rangle| = 17$ kHz (where we have suppressed the $\langle CD_3 \rangle$ superscript) and a relatively large asymmetry parameter, $\eta \approx 0.55$. These results reflect the planar reorientation of the TCTMB molecules, *i.e.* their six-fold jumps between the various possible orientations of the benzene core at the lattice sites. The magnitude of the major quadrupolar splitting is nearly one half of $v_Q^{(CD_3)}$, indicating that it corresponds to the direction normal to the molecular plane and that its sign is therefore positive, *i.e.* $\langle v_Q \rangle = +17$ kHz. This value is somewhat smaller than $\frac{1}{2}v_Q^{(CD_3)}$, most likely due to fast out-of-plane wobbling of the molecules, which further averages out the quadrupolar interaction. The fact that the biaxiality of $\langle Q \rangle$ is strongly temperature dependent, implies that the planar motion is not six-fold symmetric, *i.e.* in the jump model, not all orientations are equally populated.^{10,11}

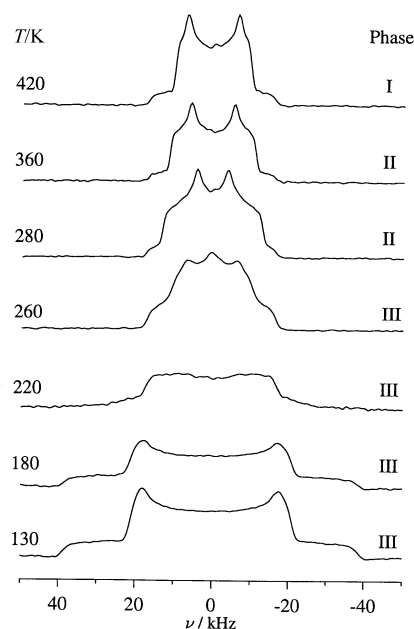


Fig. 3 Deuterium NMR spectra of a powder sample of TCTMB-d₃ as a function of the temperature, as indicated on the left. The corresponding phases are indicated on the right hand side of the figure.

Above 260 K the spectrum remains sharp and its overall width stays essentially unchanged with $\langle \nu_Q \rangle$ decreasing from 17 kHz at 260 K to 16 kHz at 420 K. This slight decrease in $\langle \nu_Q \rangle$ is probably caused by a small increase in the wobbling amplitude of the molecules. On the other hand, over the same temperature range of the measurements the asymmetry parameter gradually reduces from 0.55 to less than 0.2 (see Fig. 4), indicating a continuous change of the populations associated with the different orientations of the TCTMB molecules. Yet, although we qualitatively understand well the powder spectra over the entire temperature range of the measurements, it is not possible to derive from them quantitative data. The dynamic spectra in Phase III are a superposition of subspectra belonging to two symmetry inequivalent sites, M and M'. Their simulation would require ten adjustable parameters (two independent populations and three jump rates for each site), which is quite unfeasible to implement. Even the averaged-out spectra in Phase II, where the molecules M and M' are equivalent, cannot be quantitatively analyzed in terms of the orientation distribution of the molecules. This is so because $\langle \nu_Q \rangle$ is fixed by the model so that there is only one measured parameter, *i.e.* η , while there are two independent populations to determine. Also, no discontinuity in the line-shape is observed in the Phase III to Phase II transition, although a discontinuity is expected on the basis of the DSC and X-ray results. We therefore resort to single crystal experiments in order to get more quantitative information on the solid phases of TCTMB.

Before describing the single crystal measurements, we briefly report on a 2D-exchange experiment¹² performed on a perdeuterated powder sample of TCTMB-d₉. This experiment allows identification of the nature of the process, *i.e.* whether it involves discrete jumps (60°/120°, or other angles), or planar diffusion. The former will yield a 2D pattern with well defined, jump-angle dependent ellipsoidal ridges, while the latter will merely result in partial smearing of the main diagonal ridge. In the top part of Fig. 5, is shown such an experimental spectrum, recorded at 195 K with a mixing time of 200 ms. At this temperature there is already significant exchange broadening, resulting in severe signal loss. Nevertheless, clear ridges corresponding to 60° jumps, as may be deduced by comparison with simulation (bottom part of Fig. 5) are observed. Although this result is anticipated from the X-ray structure, it lends support to the jump model used in the interpretation of the dynamic spectra.

4.2 Deuterium NMR of Crystal A in the monoclinic Phase II

In Fig. 6 are shown deuterium NMR spectra of TCTMB-d₃, obtained from Crystal A in the monoclinic Phase II at 370 K,

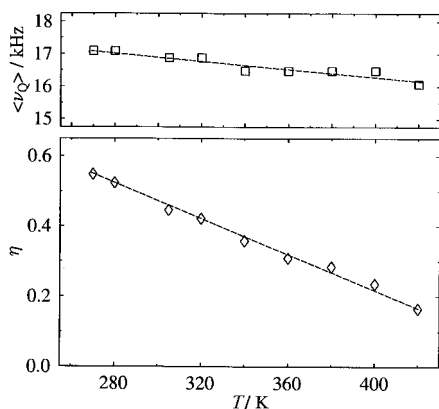


Fig. 4 Plots of the asymmetry parameter, η (bottom), and the quadrupole splitting, $\langle \nu_Q \rangle$ (top), of the TCTMB-d₃ deuterons, derived from powder spectra of the type shown in Fig. 3, as a function of the temperature.

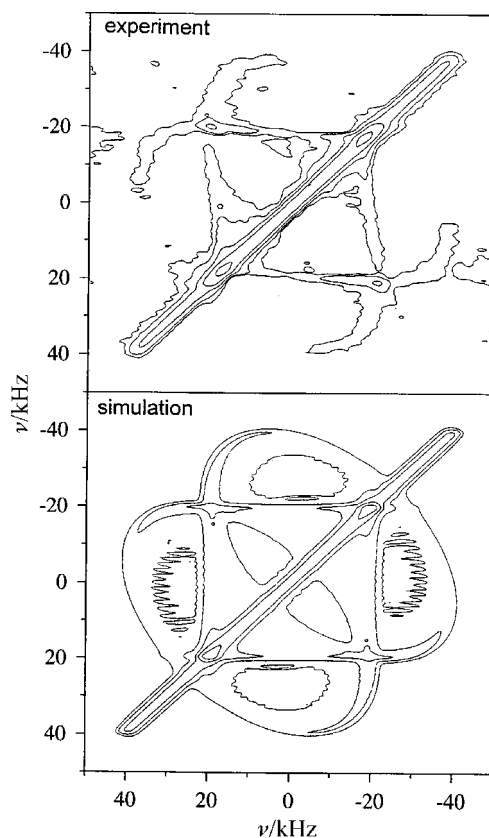


Fig. 5 Top: A deuterium 2D-exchange spectrum of a powder sample of TCTMB-d₉, at 195 K; mixing time $\tau_m = 200$ ms, 40 t_1 increments, 32 scans per increment, 10 s recycle time. Bottom: Simulated spectrum, using symmetric three-fold jumps (120°), $k\tau_m \gg 1$, $\langle \nu_Q \rangle = 40$ kHz, $1/T_2 = 2000$ s⁻¹.

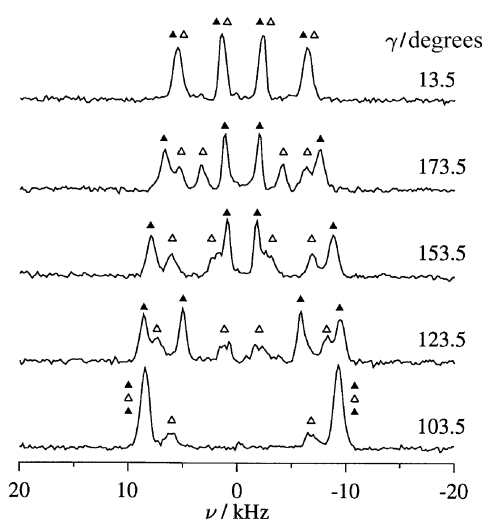
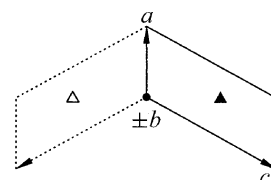


Fig. 6 Top: Schematic representation of the twinning of Crystal A; the crystallographic *a* axis is common to both twins, while the *b* axes are antiparallel. Bottom: Deuterium NMR spectra of Crystal A in the monoclinic Phase II at 370 K, for several orientations of the magnetic field (goniometer angle γ). The solid and open triangles indicate, respectively, signals due to the major and minor twin.

for a number of goniometer orientations, γ . As discussed above, in this phase, in a general orientation of the magnetic field, two doublets are expected due to the CD_3 groups in the two monoclinically related molecules, M and M'. In effect (see, for example, the spectrum for $\gamma = 173.5^\circ$), two main doublets (labeled with solid triangles), and two minor ones (open triangles) of almost one half the intensity of the former, are observed. This doubling of the number of peaks was traced back to twinning, with a major and a minor twin. By inspection of the rotation pattern we found that the two twins share a common a axis, while their b axes are antiparallel, as shown at the top of Fig. 6. To interpret the spectra we first plotted the line positions as a function of γ , identified the various families of "harmonics" using a computer sorting algorithm¹³ and finally applied the SUPERFIT program¹⁴ to derive the quadrupole coupling tensors, $\langle Q \rangle$. The best-fit rotation patterns so obtained are shown in the upper diagram of Fig. 7, where the full and dotted lines correspond, respectively, to the major and minor twins of the crystal. In computing the $\langle Q \rangle$ s we made use of the method of Tesche *et al.*¹⁵ for monoclinic crystals, where a single rotation experiment suffices to derive the quadrupole coupling tensor. This method is based on the fact that the rotation pattern of a monoclinically related molecule, say M', can count as a second rotation experiment on M, but with a goniometer axis related to the original one by the monoclinic symmetry (180° rotation about b). This method can be extended to other types of symmetries, for example local molecular symmetry.⁸ In the present case, for the final analysis of the rotation patterns we have extended the single rotation method to the twin symmetry of Crystal A. The situation now amounts to acquiring simultaneously rotation spectra from two crystals; the rotation pattern of, say, M(minor) can be considered as an extra experiment on M(major) with a goniometer axis related to the original one by a 180° rotation about the (common) crystallographic a axis (see Fig. 6). A similar relation exists between M'(minor) and M'(major). The polar angles of the effective goniometer axes for the four types of molecules in the twinned Crystal A are given in Table 2.

Similar to the powder, the spectrum of the single crystal is also temperature dependent, as reflected by the shifts of the line positions. Examples of spectra at different temperatures, within Phase II, and associated rotation patterns (actually only those for the minor twin) are shown in Fig. 8. The temperature effect is quite significant and reflects the changes in $\langle Q \rangle$ due to shifts in the population distribution in the various sites. We have analyzed the rotation patterns over the entire temperature range of Phase II as described above, and the results for the principal values of $\langle Q \rangle$ and their principal

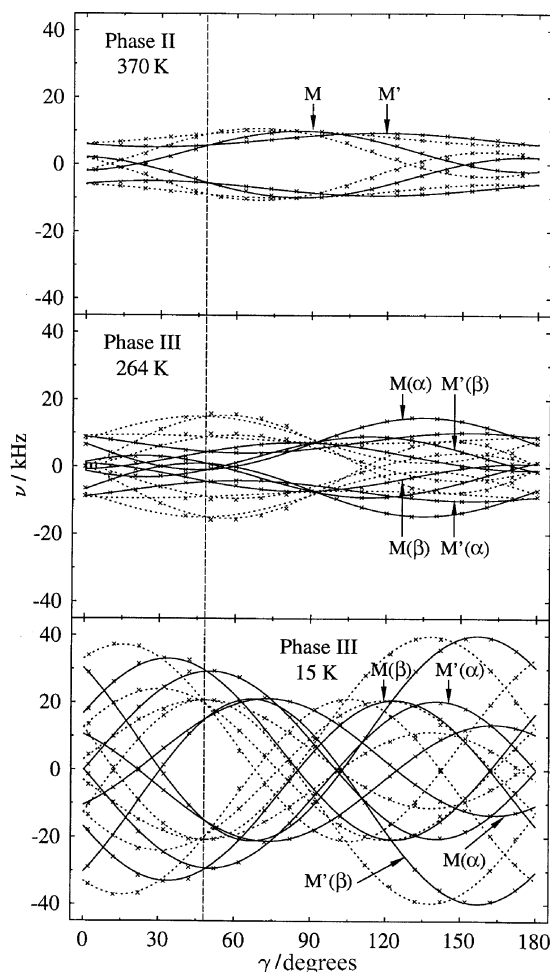


Fig. 7 Rotation patterns of Crystal A in the monoclinic Phase II (370 K) and in the triclinic Phase III, before (15 K) and after (264 K) the dynamic averaging of the quadrupole coupling tensor. The full and dotted lines correspond, respectively, to the major and minor twin. The lines of the major twin are identified with the molecules in the unit cell according to the notation of Fig. 2. The vertical dashed line corresponds to the γ value where the magnetic field crosses the ac plane.

directions (θ and ϕ in the SOS), are summarized in Table 3(a). The orientations quoted in the Table are for molecule M. Those for M' can be obtained by a 180° rotation about the crystallographic b axis ($\theta \rightarrow \pi - \theta$, $\phi \rightarrow \pi - \phi$). The identification of the M and M' tensors with the M and M' molecules was

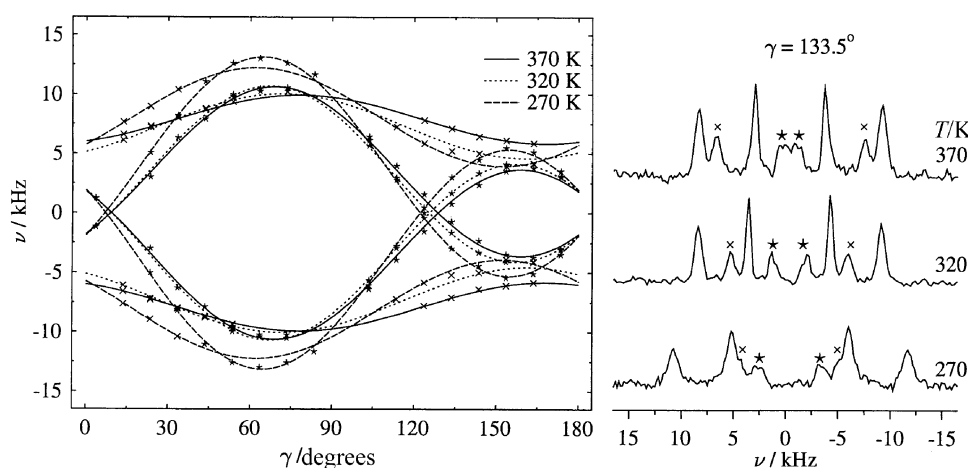


Fig. 8 Right: Deuterium NMR spectra of Crystal A at several temperatures in the monoclinic phase for a fixed goniometer angle ($\gamma = 133.5^\circ$). The stars and crosses mark the signals of the monoclinically related molecules, M and M', of the minor twin, that are plotted on the left. Left: The full rotation patterns for the signals marked on the right, for the indicated temperatures.

Table 3 The principal values $\langle Q \rangle_{ii}$ (in kHz) and principal directions d_{ii} (θ , ϕ , in the SOS), of the TCTMB-d₃ $\langle Q \rangle$ tensors, at the indicated temperatures^{a,b}

T/K	Mol.	$\langle Q \rangle_{xx}$	d_{xx}	$\langle Q \rangle_{yy}$	d_{yy}	$\langle Q \rangle_{zz}$	d_{zz}
(a) M molecules in the monoclinic phase							
270		-17.52	26.5, 168.1	-5.3	64.1, 335.3	22.82	84.9, 67.8
280		-17.35	23.7, 169.7	-5.55	66.9, 335.7	22.90	84.9, 67.9
300		-16.58	21.0, 170.3	-6.21	69.6, 336.3	22.79	85.3, 68.0
320		-14.38	18.7, 172.5	-6.22	72.0, 336.2	20.60	85.1, 67.8
340		-15.25	17.2, 172.4	-7.24	73.3, 336.9	22.49	85.6, 68.2
360		-14.65	15.2, 173.1	-7.77	75.4, 337.1	22.42	86.0, 68.1
370		-14.39	13.9, 174.1	-7.94	76.7, 337.3	22.33	86.1, 68.2
(b) M(α) and M(β) molecules in the triclinic phase							
255	M(α)	-15.69	90.2, 337.1	-7.40	5.6, 249.2	23.09	84.4, 67.0
	M(β)	-23.81	133.0, 344.2	1.12	44.4, 326.6	22.69	81.1, 65.1
258	M(α)	-14.93	95.6, 336.8	-8.19	8.0, 290.6	23.12	84.3, 66.2
	M(β)	-22.77	134.1, 344.3	0.73	45.1, 328.6	22.04	82.1, 66.6
261	M(α)	-14.20	101.9, 337.5	-8.83	13.3, 310.6	23.03	84.1, 66.2
	M(β)	-21.64	44.3, 164.4	-0.25	46.6, 329.7	21.89	82.6, 66.8
264	M(α)	-13.53	115.9, 339.1	-9.40	26.7, 324.7	22.93	84.2, 66.3
	M(β)	-20.50	42.7, 164.2	-1.45	48.1, 330.0	21.95	82.9, 66.4

^a The principal directions of the monoclinically related molecules are obtained by a 180° rotation about the crystallographic *b* axis. ^b The estimated errors of the principal values and directions are, respectively, ± 0.2 kHz and $\pm 0.4^\circ$.

based on the assumption that the directions of the major principal axes (d_{zz} in Table 3(a)) must coincide with those of the corresponding normals to the molecular planes (\perp in Table 1). Likewise, the signs of the quadrupole tensor components in Table 3(a) are based on the assumption that the major component, $\langle Q \rangle_{zz}$, must have the same sign as the perpendicular component of $\mathbf{Q}^{\langle \text{CD}_3 \rangle}$, and is therefore positive, as discussed for the powder spectrum. The principal values of $\langle Q \rangle$ are also plotted as a function of the temperature in Fig. 9. These results are fully consistent with those for the powder (Fig. 4). In particular, $\langle v_Q \rangle$ and η of the powder match, respectively $\frac{3}{4}\langle Q \rangle_{zz}$ and $(\langle Q \rangle_{yy} - \langle Q \rangle_{xx})/\langle Q \rangle_{zz}$, of the single crystal results (note the use of lower case subscripts for the average tensor components). The latter include, however, also the orientation of the average tensors, which is crucial for the population analysis to be described in the next section.

4.3 Population analysis in Phase II

As discussed in the above section, the measured quadrupole tensors in Phase II, $\langle Q \rangle$, are averages over the various orientations (directions of the associated arrows) of the TCTMB molecules in the lattice. Thus,

$$\langle Q \rangle = \sum P_i \mathbf{Q}_i^{\langle \text{CD}_3 \rangle} \quad (1)$$

where P_i is the fractional population of orientation i and $\mathbf{Q}_i^{\langle \text{CD}_3 \rangle}$ is the corresponding quadrupolar tensor of the (rapidly reorienting) methyl group. In the present section we analyze the $\langle Q \rangle$ s and their temperature dependence in terms of the fractional populations of the molecules at the various orientations. To do so we derive an expression for $\langle Q \rangle$ based on eqn. (1), and then compare it with the experimental results at each temperature.

For TCTMB there are six possible molecular orientations (arrows) at a crystal site, which we label 1, 2, 3, 1', 2' and 3' (see top of Fig. 10). However, since the orientations 1–1', 2–2' and 3–3' are pairwise related by inversion symmetry, they are also pairwise magnetically equivalent, $\mathbf{Q}_i^{\langle \text{CD}_3 \rangle} = \mathbf{Q}_{i'}^{\langle \text{CD}_3 \rangle}$, and their fractional populations are identical, $p_i = p_{i'}$. Thus, in eqn. (1), the summation runs from $i = 1$ to 3 and the P_i s now stand for the population sums, $P_i = p_i + p_{i'}$. To use eqn. (1) correctly, the various $\mathbf{Q}_i^{\langle \text{CD}_3 \rangle}$ s must be written in a common coordinate system. We choose this to be the principal axis system (PAS) of orientation 1 of molecule M, as defined in the upper part of Fig. 10, with *x* along the 1-direction, *z* along the

normal to the molecular plane and *y* completing the set to a right-handed system. We refer to this coordinate system as the averaging axis system (AAS). Also, we assume that the $\mathbf{Q}_i^{\langle \text{CD}_3 \rangle}$ s are axially symmetric with $Q_{\parallel}^{\langle \text{CD}_3 \rangle} = Q_{zz}^{\langle \text{CD}_3 \rangle} = \chi$ and

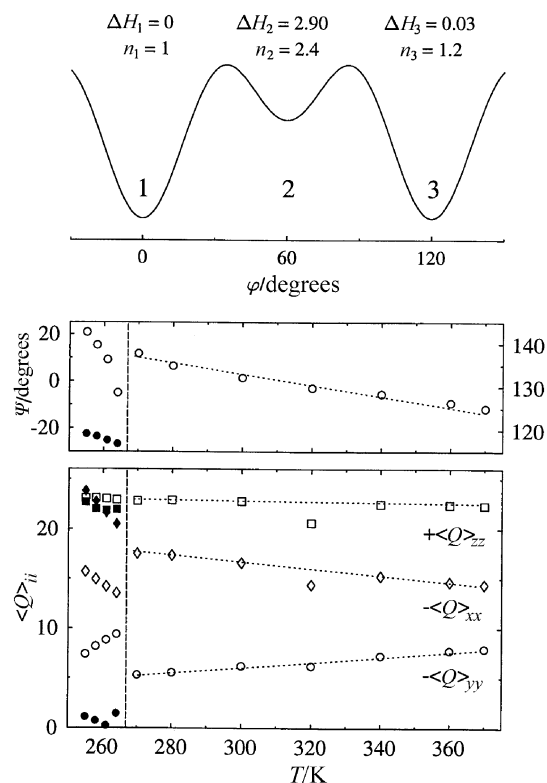


Fig. 9 Top: Schematic potential energy diagram for the three-fold (six-fold) planar jumps of the TCTMB molecules in the monoclinic Phase II. The inserted numbers are the fitted enthalpies (kJ mol⁻¹) and degeneracies (eqn. (9)) for the corresponding sites. Bottom: The principal values of the quadrupole coupling tensor, $\langle Q \rangle$. ψ is the angle between the direction associated with $\langle Q \rangle_{xx}$ and the direction of substituent 1 (*x*-component of the AAS) as defined in Fig. 10. Both quantities are plotted as a function of the temperature in Phase II and the upper temperature region of Phase III (respectively, right and left of the vertical dashed line at 268 K). The open and solid symbols in Phase III refer to molecules M(α), M(β), and M(β), M'(α) respectively. Note the different ψ -scale for the two phases.

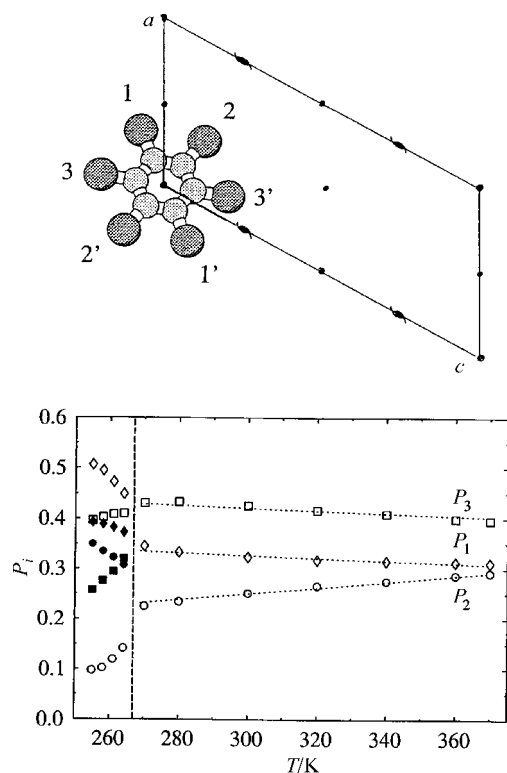


Fig. 10 Top: Labeling of the substituent orientations of the TCTMB molecule. The labels apply to molecule M of the monoclinic cell of Phase II and to the molecules M(α) and M(β) of the triclinic supercell of Phase III. Bottom: The calculated fractional populations, P_1 , P_2 and P_3 in the monoclinic Phase II and the upper temperature range of Phase III (respectively, right and left of the vertical dashed line at 268 K). In the latter phase the open symbols refer to the M(α), M(β) molecules, while the solid symbols to the M(β), M'(α) molecules. The dotted lines are calculated using eqn. (9) and the thermodynamic parameters given at the top of Fig. 9.

$Q_1^{\langle CD_3 \rangle} = -\frac{1}{2}\chi$, so that

$$\mathbf{Q}_1^{\text{AAS}} = \mathbf{Q}_1^{\langle CD_3 \rangle} = \chi \begin{pmatrix} 1 & & \\ & -\frac{1}{2} & \\ & & -\frac{1}{2} \end{pmatrix} \quad (2)$$

The corresponding tensors of orientations 2 and 3 in the AAS are obtained by a "passive" rotation¹⁶ of their respective PAS coordinates into the PAS of orientation 1,

$$\mathbf{Q}_i^{\text{AAS}} = R(\varepsilon_i) \mathbf{Q}_i^{\text{PAS}} R(\varepsilon_i)^{-1} = \frac{\chi}{2} \begin{pmatrix} (3 \cos^2 \varepsilon - 1) & -3 \cos \varepsilon \sin \varepsilon & 0 \\ -3 \cos \varepsilon \sin \varepsilon & (3 \sin^2 \varepsilon - 1) & 0 \\ 0 & 0 & -1 \end{pmatrix} \quad (3)$$

where

$$R(\varepsilon) = \begin{pmatrix} \cos \varepsilon & \sin \varepsilon & 0 \\ -\sin \varepsilon & \cos \varepsilon & 0 \\ 0 & 0 & 1 \end{pmatrix} \quad (4)$$

and ε is $+60^\circ$ for substituent 2 and -60° for substituent 3 (*cf.* Fig. 10). This gives

$$\mathbf{Q}_2^{\text{AAS}} = \frac{\chi}{8} \begin{pmatrix} -1 & -3\sqrt{3} & 0 \\ -3\sqrt{3} & 5 & 0 \\ 0 & 0 & -4 \end{pmatrix} \quad (5)$$

$$\mathbf{Q}_3^{\text{AAS}} = \frac{\chi}{8} \begin{pmatrix} -1 & 3\sqrt{3} & 0 \\ 3\sqrt{3} & 5 & 0 \\ 0 & 0 & -4 \end{pmatrix}$$

Inserting in eqn. (1) yields

$$\langle \mathbf{Q}^{\text{AAS}} \rangle = \frac{\chi}{8} \begin{pmatrix} (-1 + 9P_1) & & & \\ 3\sqrt{3}(1 - P_1 - 2P_2) & & & \\ & 3\sqrt{3}(1 - P_1 - 2P_2) & 0 & \\ & (5 - 9P_1) & 0 & \\ & 0 & 0 & -4 \end{pmatrix} \quad (6)$$

To compute the P_i s the tensor of eqn. (6) must be compared with the experimentally determined tensor (Table 3(a), Fig. 9). As above, both tensors must be written in the same coordinate system, and we again choose the AAS, *i.e.*, we need to transform the experimental $\langle \mathbf{Q} \rangle$ from its PAS (Table 3(a)) to the AAS.

Inspection of the results in Table 3(a) shows that the magnitude of the major component of $\langle \mathbf{Q} \rangle$, $\langle Q \rangle_{zz}$, is essentially independent of the temperature (~ 22.5 kHz) and similar to the perpendicular component of $\mathbf{Q}^{\langle CD_3 \rangle}$ ($Q_1^{\langle CD_3 \rangle} = -\frac{1}{2}\chi$). Also, its orientation ($\theta, \phi \sim 85^\circ, 68^\circ$) does not change with the temperature and is essentially parallel to the molecular plane normal, *i.e.* along z of the AAS (*cf.* Table 1). Thus, only a single (passive) rotation about the molecular normal axis is needed to transform the experimental $\langle \mathbf{Q} \rangle$ from its PAS to the AAS,

$$\langle \mathbf{Q}^{\text{AAS}} \rangle = R(\psi) \langle \mathbf{Q} \rangle R(\psi)^{-1} = \begin{pmatrix} \langle Q \rangle_{xx} \cos^2 \psi + \langle Q \rangle_{yy} \sin^2 \psi & & & \\ -\langle Q \rangle_{xx} + \langle Q \rangle_{yy} \sin \psi \cos \psi & & & \\ & 0 & & \\ -\langle Q \rangle_{xx} + \langle Q \rangle_{yy} \sin \psi \cos \psi & 0 & & \\ \langle Q \rangle_{xx} \sin^2 \psi + \langle Q \rangle_{yy} \cos^2 \psi & 0 & & \\ & 0 & \langle Q \rangle_{zz} & \end{pmatrix} \quad (7)$$

where ψ is the angle between the eigenvector associated with $\langle Q \rangle_{xx}$ (Table 3(a)) and the x direction in the AAS. The experimental values of ψ , so obtained, are included in Fig. 9. Finally, to determine the populations, we compare the tensors of eqn. (6) and eqn. (7) element by element and (recalling that $\Sigma P_i = 1$) extract the following expressions,

$$P_1 = \frac{1}{9} \left[1 - \frac{8}{2\langle Q \rangle_{zz}} (\langle Q \rangle_{xx} \cos^2 \psi + \langle Q \rangle_{yy} \sin^2 \psi) \right]$$

$$P_2 = \frac{1}{2} \left[1 - P_1 + \frac{8}{6\sqrt{3}\langle Q \rangle_{zz}} (-\langle Q \rangle_{xx} + \langle Q \rangle_{yy}) \sin \psi \cos \psi \right]$$

$$P_3 = 1 - P_1 - P_2 \quad (8)$$

where we substituted $\chi = -2\langle Q \rangle_{zz}$. Inserting the experimental values of ψ and of the components of $\langle \mathbf{Q} \rangle$ (Table 3(a)), yields the populations, P_i , plotted in the bottom part of Fig. 10.

It may be seen that these plots do not obey a simple Boltzmann behavior based on enthalpy alone, as reflected in the fact that the three populations do not approach a common high-temperature asymptotic value of 1/3. Clearly, entropy factors affect the population distribution and accordingly we fit the population curves to the more general equation

$$P_i = \frac{[\exp(T\Delta S_i - \Delta H_i)/RT]}{\sum [\exp(T\Delta S_i - \Delta H_i)/RT]} = \frac{n_i \exp(-\Delta H_i/RT)}{\sum n_i \exp(-\Delta H_i/RT)} \quad (9)$$

where $n_i = \exp(\Delta S_i/R)$ is a measure of the site degeneracy. Setting, arbitrarily, the enthalpy and degeneracy of orientation 1, to $\Delta H_1 = 0$ and $n_1 = 1$, we obtain the values inserted at the top of Fig. 9. This insert also includes a schematic potential

energy diagram, based on the population analysis results. It shows that orientations 1 and 3 have similar local potential minima, while orientation 2 is less stable and appears to be more highly degenerate.

An important conclusion from this analysis is that Phase II has no complete planar disorder, as suggested by the X-ray results.⁴ Rather, a population difference between the different orientations is maintained even at high temperatures. As the temperature is lowered, orientation 2 becomes depleted, while the populations of orientations 1 and 3 increase. It is tempting to ascribe this increase in polarization as a pretransition effect, as if the system anticipates the polarization in Phase III. We discuss this point in the next section. As will be seen, this anticipation is only partly fulfilled.

4.4 Deuterium NMR and population analysis in the triclinic Phase III

As discussed in Section 2, the transition from the monoclinic Phase II to the triclinic Phase III, although first order, does not involve displacements of the molecules or any major change in their tilt. According to the X-ray results the transition involves predominantly the setting-in of spontaneous polarization. The two originally symmetry related molecules, M and M' of Phase II now become inequivalent, in the sense that they polarize in different orientations and to different degrees. Thus, upon transition to Phase III, the signals associated with the M molecules of Phase II split into a pair of symmetry unrelated signals, M(α) and M(β), while those of M' yield the pair M'(α) and M'(β). From the discussion of Section 2, it also follows that the pair M(α), M'(β) is monoclinically related and likewise the pair M(β), M'(α).

In Fig. 11 (top) are shown two spectra of Crystal A, recorded just above (270 K) and below (260 K) the II \leftrightarrow III phase transition temperature (268 K). The magnetic field orientation was such that the monoclinically related molecules are magnetically inequivalent. Hence, two well resolved doublets are observed (for the major twin) in Phase II and four barely resolved doublets in Phase III, as expected from the above discussion. Such "narrow-lined" spectra as shown in the 260 K trace of Fig. 11, are observed only over a very limited temperature range of Phase III, from 268 K down to about 255 K. Below this temperature, the system enters the dynamic NMR regime: The lines first broaden and, on further cooling, narrow again. Below 180 K, a new high-resolution spectrum emerges (see the 160 K trace in Fig. 11), where the molecular reorientation is frozen out, but not the reorientation of the methyl groups. The spectrum then remains essentially unchanged down to about 15 K. We will delay the discussion of the dynamic effects to a later section. Here we limit ourselves to the two regimes of extreme fast and extreme slow molecular reorientation in Phase III.

In the upper temperature range (255 to 268 K) there is a rapid six-fold jump process of the TCTMB molecules between unequally populated orientations, leading to average biaxial tensors, as in Phase II. Since, however, in Phase III the monoclinic pair M(α), M'(β) is symmetry unrelated to the M(β), M'(α) pair, two different tensors reflecting the different population distribution in the two type of sites are expected. To determine the populations, four rotation experiments, at different temperatures in the range 255 to 268 K, were performed. One such rotation pattern, corresponding to 264 K, is shown in the middle part of Fig. 7. Following the identification of the monoclinically related pairs (pairwise crossing when the magnetic field traverses the *ac* plane), the analysis proceeded as for the Phase II spectra. The results, so obtained, are summarized in Table 3(b) and in Fig. 9. The identification of the quadrupolar coupling tensors of the two inequivalent pairs with the crystal sites M(α), M'(β) or M(β), M'(α) cannot be done in an unequivocal fashion. This is so, because the molecular plane

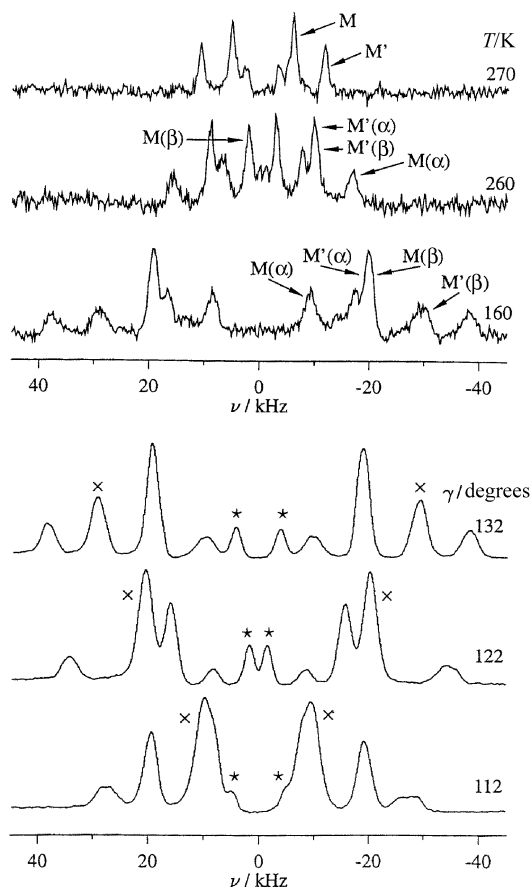


Fig. 11 Selected deuterium NMR spectra of Crystal A. Top: Spectra recorded at a fixed orientation of the magnetic field ($\gamma = 133.5^\circ$) at the indicated temperatures. The peak labeling refers to the molecules of the major twin. Bottom: Spectra recorded at 15 K for a number of crystal orientations, as indicated. The crosses and stars label M'(β) and M(α) molecules of the major twin.

normals of the symmetry unrelated molecules, *e.g.* M(α) and M(β) are essentially parallel and can therefore not be used for their identification. We shall shortly return to this problem, and meanwhile adopt the assignment of Table 3(b) and Fig. 9.

Once the $\langle Q \rangle$ s of the two pairs of sites were determined, we calculated the orientation populations, as described for the monoclinic Phase II. The situation here is, however, somewhat more subtle. In the triclinic phase the molecules do not occupy sites of inversion symmetry. Consequently p_i need not be identical to $p_{i'}$ so that, in principle, there are six populations for each crystal site. It may be seen, however (see Fig. 2), that in the triclinic lattice, down the b_1 axis, the molecules are alternately related by inversion symmetry, so that within a unit cell, $p_i = p_{i'}$. Since the NMR spectra of inversion related sites are identical, we can only detect their sum $P_i = p_i + p_{i'}$, and the problem reduces again to that of the monoclinic Phase II (eqn. (8)). The results so obtained are plotted in Fig. 10, together with those for Phase II. We thus see that Phase III is also disordered, at least in its upper temperature range with unequal populations for the various substituent directions.

At low temperatures (< 100 K) this phase indeed becomes fully polarized with only one orientation populated for each site. This follows from the analysis of rotation patterns recorded in this temperature range. One such rotation pattern, recorded at 15 K, is shown at the bottom of Fig. 7. An identical rotation pattern was obtained at 100 K. Analysis of these results gave the principal values and principal directions summarized in Table 4. The resulting tensors correspond essentially to static molecules with rapidly reorienting methyl

Table 4 Principal values $Q_{ii}^{<CD_3>}$ (in kHz) and principal directions d_{ii} (θ , ϕ , in the SOS) of the $\mathbf{Q}^{<CD_3>}$ tensors for the M(α) and M(β) molecules in the triclinic phase, as determined from rotation experiments at 15 K. Also given are the directions of the C–CD₃ bonds (in the rows labeled Z) and the normals to the molecular planes (rows labeled Y), as determined from X-ray data at 173 K^a

<i>i</i>	Mol.	$Q_{ii}^{<CD_3>}$	d_{ii} (NMR)	d_{ii} (X-ray)	δ^b
Z	M(α)	–53.60	109.5, 334.9	110.4, 341.1	5.9
X	M(α)	28.26	19.6, 339.0	—	—
Y	M(α)	25.34	91.3, 65.4	83.9, 68.8	8.2
Z	M(β)	–53.28	52.6, 329.2	51.3, 334.2	4.1
X	M(β)	27.68	39.3, 170.1	—	—
Y	M(β)	25.60	79.6, 67.2	83.3, 69.6	4.4

^a The estimated error of the principal values is ± 0.4 kHz, and of the major principal direction $\pm 0.4^\circ$. ^b Angle between corresponding directions, obtained from the NMR and X-ray results.

groups, $\mathbf{Q}^{<CD_3>}$. The directions associated with their major principal components (parallel to the C–CD₃ bond) are now along substituent 1 for the M(α),M(β) pair and along substituent 2 for the M(α),M(β) pair (*cf.* Table 4). These directions were found to be the polarization directions in the X-ray study (see Table 1). In fact, we matched the experimental $\langle \mathbf{Q} \rangle$ s to the molecular sites by identifying their major principal directions with those of the X-ray polarizations.

We now return to the population results in the high temperature range of Phase III (Fig. 10). Referring first to the open symbols, we note that the most populated orientation for this type of molecules is P_1 (diamonds) and that, over the narrow range where measurements could be carried out, P_1 keeps increasing with decreasing temperature, at the expense of the populations of orientations 2 (circles) and 3 (squares). It is therefore natural to associate these results with those molecules in the crystal, which according to the low-temperature X-ray measurements are polarized along the 1-direction. Hence, the assignment of the open symbols to the M(α),M(β) molecules (see Fig. 2 and Table 1). The situation for the solid symbols is more complex. By elimination, we identify them with the M(α),M(β) molecules, which according to the X-ray results are, at low temperatures, polarized along the 2-direction. Indeed, P_2 of the solid symbols (Fig. 10) increases on lowering the temperature, however, the plots also show that P_1 is larger than P_2 and it also increases with temperature, at least over the narrow range of measurements. We must therefore assume that in some temperature range within Phase III, P_1 of the M(α),M(β) molecules passes through a maximum and then decreases on further cooling. This behavior is not consistent with a regular Boltzmann equation, which predicts a monotonic change in population with temperature. A way out of this dilemma is to assume that the packing potential in which the TCTMB molecules are embedded, is temperature dependent, *e.g.* by the gradual changes in polarization with the temperature. It would be interesting to confirm this assumption by measuring the populations over the entire range of Phase III. Unfortunately, this is not possible by the technique described above, because of the smearing out of the signals due to dynamic line broadening.

Before concluding this section we wish to comment on some line intensity peculiarities, observed in the low-temperature region of Phase III. Examples of such spectra of the twinned Crystal A, are shown at the bottom of Fig. 11. These spectra, which include the peak assignments, were recorded at 15 K, for several γ values. Close inspection of the spectra reveals that pairs of doublets, which are related by the pseudo-monoclinic symmetry, do not have identical intensities. For example, it may be seen in the $\gamma = 132^\circ$ trace that the intensity of the doublet due to the M(β) molecules of the major twin (crosses) is quite different from that of the M(α) molecules (stars). Similar anomalies are observed for the other

monoclinic pair of doublets, as well as in the two doublets of the minor twin (not labeled in the figure). These anomalies are not always readily detected, because most spectra suffer from excessive line overlap. For the spectra shown in Fig. 11, we can safely rule out experimental artifacts, such as saturation, and we believe that the effect is real. We recall that the pseudo-monoclinic symmetry of Phase III stems from the assumption of equal number of α and β domains in the sample. This assumption is, however, not required by any symmetry or thermodynamic consideration. It is likely that for melt-grown crystals, as used in our NMR measurements, the distribution of the α and β domains is not statistical, leading to the observed intensity difference.

4.5 Dynamic effects: Line broadening and T_1 relaxation

In the temperature range 180 to 260 K, the deuterium NMR spectra of TCTMB-d₃ exhibit line broadening effects, reflecting the molecular six-fold jumps within the lattice sites. In Fig. 12 (left) two sequences of experimental spectra, for the single Crystal A (top) and for a powder sample (bottom) are shown. The spectra exhibit characteristic dynamic features that in principle could be simulated by standard dynamic NMR methods. The application of these methods to the present problem is, however, quite demanding. As already indicated the simulations require a total of ten adjustable parameters (three rate constants and two fractional populations for each site). Nevertheless, we made a crude attempt to simulate the spectra by assuming, (a) $k_{12} = k_{23} = k_{13} = k$ (where k_{ij} is the rate constant for the jump from orientation j to orientation i), (b) identical rates for the two symmetry unrelated molecules and (c) a Boltzmann equation for the populations of the form,

$$P_i = n_i \exp(-E_i/RT)/Z \quad (10)$$

where Z is the partition function. The parameters, n_i and E_i for each orientation were determined from two sets of populations at the high and low temperature limits of the simulation range. At the high temperature end (260 K) the experimental P_i s from Fig. 10, were taken, while at the low temperature end (100 K), the populations of the polarized orientations (P_1 [M(α)], P_1 [M(β)] and P_2 [M(α)], P_2 [M(β)] were chosen to be 0.90, and all other P_i s were set to 0.05. The latter assumption is consistent with the restriction that the line broadening cannot exceed the order of $P_i \cdot \langle \mathbf{Q} \rangle$. Using these assumptions and an exchange independent linewidth of $1/T_2^* = 5000 \text{ s}^{-1}$, the simulated lineshapes shown on the right-hand side of Fig. 12, were obtained. Although the spectra reproduce many of the experimentally observed features, the fit is far from perfect, clearly due to the over-simplified model used. An Arrhenius plot of the “best-fit” rate

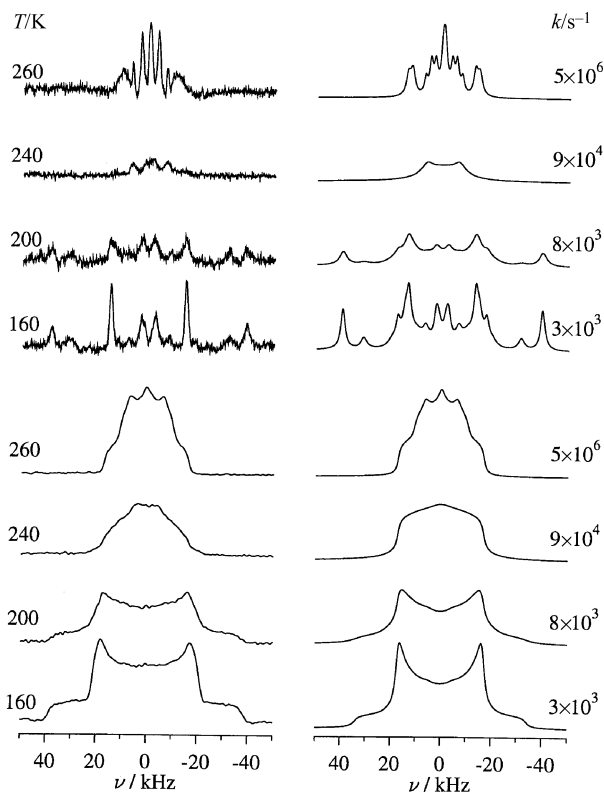


Fig. 12 Left: Experimental deuterium NMR spectra of Crystal A at a goniometer angle of $\gamma = 160^\circ$ (four upper traces) and of a powder sample of TCTMB- d_3 (four bottom traces), at the indicated temperatures. Right: Simulated spectra calculated, using assumptions described in the text and the indicated rate constants for planar three fold molecular jumps.

constants yields the kinetic parameters shown in the first row of Table 5.

Complementary dynamic information can be derived from relaxation data. The deuterium longitudinal relaxation times of TCTMB- d_3 were measured on two specimens; a powder sample in the temperature range 160 to 400 K, and a single crystal (Crystal B), in the range 10 to 55 K. The results for both samples are plotted in Fig. 13. We defer the discussion of the low temperature data to a later section. The T_1 results of the powder sample correspond, at the higher temperature range, to the outer shoulders (parallel features) of the spectra, at around ± 17 kHz, which at lower temperatures turn into the perpendicular horns of the powder pattern. These results thus apply to those molecules in the powder whose plane normals lie parallel to the external magnetic field. They cover the temperature range of the two phases III and II, with a

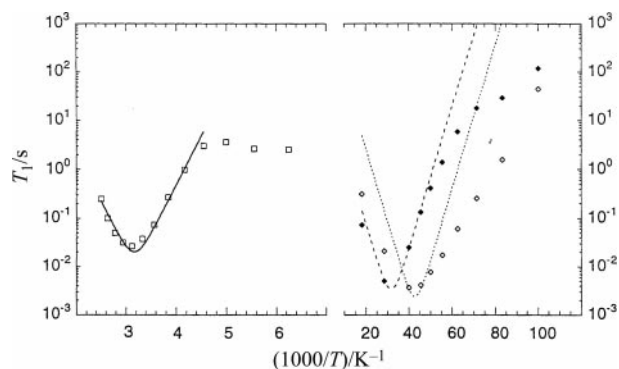


Fig. 13 Longitudinal relaxation times, T_1 , of the deuterons in TCTMB- d_3 as a function of the temperature. The high-temperature results (open squares) were obtained on a powder sample and correspond to the shoulders (at low temperatures, horns) at $\nu = \pm 17$ kHz (magnetic field perpendicular to the molecular planes). The low-temperature results were obtained on Crystal B. The open and solid diamond symbols correspond, respectively, to molecules $M(\alpha), M'(\beta)$ and $M(\beta), M'(\alpha)$. The various lines are calculated using equations given in the text and the appropriate kinetic parameters shown in Table 5.

clear T_1 minimum at around 320 K. No discontinuity is observed at the phase transition. The T_1 relaxation around this minimum is clearly dominated by the planar six-fold (actually, three-fold) jumps of the TCTMB molecules and can be analyzed using suitable relaxation equations. To simplify the analysis we assume identical populations and equal jump rates, k , between all orientations. In view of our earlier discussion, these are, admittedly, very crude assumptions, but they are acceptable in the temperature range of the analysis and they make the problem tractable. Under these conditions the deuterium relaxation rate in the TCTMB- d_3 molecules becomes,¹⁷

$$\frac{1}{T_1} = (2\pi\nu_Q^{\langle CD_3 \rangle})^2 \left(\frac{\tau_c}{1 + 4\omega_0^2 \tau_c^2} \right) \quad (11)$$

where $\tau_c = 1/3k$. Fitting eqn. (11) to the high temperature results of Fig. 13, and assuming an Arrhenius temperature dependence for k , the kinetic parameters shown in the second row of Table 5 were obtained. As may be seen they are quite close to those estimated from the lineshape fitting.

These results are also of the same order of magnitude as estimated earlier by several other groups. For example, the proton NMR linewidth measurements by Brot *et al.*⁶ show a characteristic dispersion at around 223 K, which has been interpreted as due to molecular reorientation. Using the experimental results in this paper, we estimate the rate constant entered in the third row of Table 5. The activation energy shown in the same line, was derived from a subsequent

Table 5 Kinetic parameters for the reorientational jumps and of the incoherent methyl group reorientation in solid TCTMB

Dynamic mode	Method	$E_a/\text{kJ mol}^{-1}$	k/s^{-1} (T/K)	Ref.
Planar reorientation	^2H , lineshape	41.0	5×10^6 (260)	this work
	^2H , T_1	38.5 ± 0.5	7×10^6 (260)	this work
	^1H , linewidth	40.0^a	9×10^4 (223) ^b	6
	^1H , T_1	52.0^c	$\approx 10^8$ (300) ^d	7
	dielectric relax.	— ^e	3×10^5 (226)	1
	dielectric relax.	42.7^c	— ^e	3
Methyl reorientation	^2H , T_1	2.8 ± 0.3	1×10^9 (25)	this work
	^1H , T_1	2.1	— ^e	7

^a From the Thesis of I. Darmon (Paris, 1969), quoted by Chezeau *et al.*⁷ ^b Estimated from the midpoint of the dispersion curve. ^c A distribution of correlation times was assumed in the analysis. ^d Estimated from the T_1 minimum. ^e Not given.

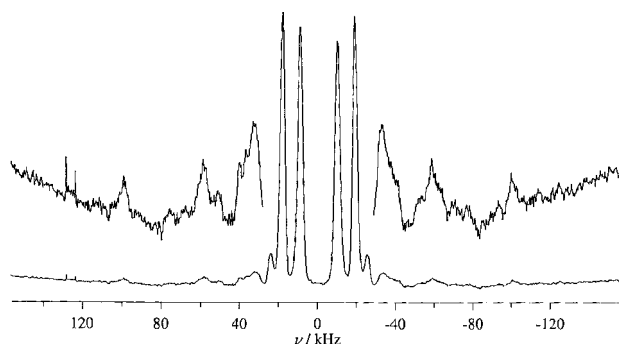


Fig. 14 A deuterium NMR spectrum of Crystal B at 12 K. The upper trace is plotted at an 8-fold gain in order to enlarge the “tunneling peaks” at the outer wings of the spectrum.

analysis of these wide line measurements, as quoted by Chezeau *et al.*⁷ Proton relaxation-time measurements by the latter group⁷ gave a characteristic T_1 minimum at 290 K, which was also ascribed to planar molecular reorientation. From these data they derived the activation energy listed in the fourth row of Table 5. It is interesting that the authors, not being able to quantitatively fit the relaxation data to a single rate constant, concluded that the motion involves a distribution of correlation times. This probably reflects the inequivalency of the various sites, as discussed above. Finally, we mention the dielectric relaxation data of White *et al.*¹ and of Brot *et al.*,³ (fifth and sixth row of Table 5), who also claim that the process involves a distribution of correlation times. It is remarkable that despite the crudeness of the models used in the interpretation of the various experiments, the resulting kinetic parameters are pretty similar.

4.6 Classical reorientation and coherent quantum-mechanical tunneling of the methyl groups

Below 100 K the deuterium NMR lineshape of the TCTMB- d_3 crystals remains essentially unchanged on further cooling down to about 15 K. Below this temperature new lines appear in the spectrum, that indicate the onset of coherent quantum-mechanical tunneling.¹⁸ Well before this temperature range, at around 170 K, the T_1 relaxation time begins to shorten due to slowing down of the classical, incoherent, reorientation of the CD_3 groups. In the present section we briefly address these two phenomena.

On the right-hand side of Fig. 13 are plotted T_1 results obtained on a single crystal (Crystal B) of TCTMB- d_3 , in the temperature range 10 to 55 K. The goniometer axis for this crystal was mounted along the crystallographic b axis, so that for all rotation spectra the magnetic field lies in the ac plane. Hence, all spectra consist of just two doublets, due to the two sets of crystallographically inequivalent molecules, $M(\alpha), M(\beta)$ and $M(\beta), M(\alpha)$. For the T_1 relaxation measurements, the orientation of the magnetic field was such that it subtended 27.1° and 79.3° with the C- CD_3 bonds of the $M(\alpha), M(\beta)$ and $M(\alpha), M(\beta)$ molecules, respectively. The two T_1 curves in Fig. 13 correspond to these two types of molecules. Both sets of data pass through a minimum at, respectively, 30 and 24 K. These results reflect the slowing down of the reorientation of the CD_3 groups and can be used to derive kinetic parameters for this process. The general equation for the T_1 relaxation of a deuterium, with axially symmetric quadrupole splitting, ν_Q^{CD} , undergoing three-fold jumps between equally populated sites is,¹⁷

$$\frac{1}{T_1} = \frac{(2\pi\nu_Q^{CD})^2}{8} \left[g_1 \frac{\tau_c}{1 + \omega_0^2 \tau_c^2} + g_2 \frac{\tau_c}{1 + 4\omega_0^2 \tau_c^2} \right] \quad (12)$$

where, as before, $\tau_c = 1/3k$, and

$$\begin{aligned} g_1 &= \sin^2 2\theta(\cos^2 \vartheta + \cos^2 2\vartheta) \\ &+ \sin^4 \theta(\sin^2 \vartheta + \frac{1}{4} \sin^2 2\vartheta) \\ &- 8(\sin^3 \theta \cos \theta \sin^3 \vartheta \cos \vartheta) \cos 3\varphi \\ g_2 &= 4 \sin^2 2\theta(\sin^2 \vartheta + \frac{1}{4} \sin^2 2\vartheta) \\ &+ \sin^4 \theta(1 + 6 \cos^2 \vartheta + \cos^4 \vartheta) \\ &+ 8(\sin^3 \theta \cos \theta \sin^3 \vartheta \cos \vartheta) \cos 3\varphi \end{aligned} \quad (13)$$

In these equations, θ is the angle between the CD bond and the methyl C_3 axis, ($\theta = 70.53^\circ$, the tetrahedral angle), and ϑ/φ are the polar/azimuthal angles of the magnetic field in the principal axis system of the methyl group. Since the azimuthal orientations of the methyl deuterons are unknown, we neglected the φ -dependent term (which contributes at most $\pm 20\%$ to T_1).¹⁷ Substituting the above quoted values of ϑ and θ , we obtain the following values for g_1 and g_2 , for the two sites, $M(\alpha), M(\beta)$: $g_1 = 0.675$, $g_2 = 5.70$; $M(\alpha), M(\beta)$: $g_1 = 1.485$, $g_2 = 2.19$. Using these coefficients and fitting the experimental data of Fig. 13 to eqn. (12), yielded similar kinetic parameters for the two independent molecules. In the final analysis we performed a common fit to both sets of data and the results are given in the penultimate row of Table 5. The result for the activation energy is in agreement with that of Chezeau *et al.*,⁷ obtained from proton relaxation experiments (see last entry in Table 5).

On the basis of the above kinetic results we would expect the deuterium spectrum of TCTMB- d_3 to start broadening on cooling below 20 K, due to the freezing out of the thermally activated methyl group reorientation. In fact, this does not happen. Instead the spectra acquire a new structure, manifested in the appearance of typical tunneling peaks. A spectrum, recorded at 12 K, where such extra peaks are clearly observed, is shown in Fig. 14. In the present work we have not attempted a quantitative analysis of the TCTMB- d_3 tunneling spectra. Qualitatively, however, they clearly indicate that below about 15 K, the CD_3 groups decouple from the lattice thermal bath and enter a regime of coherent tunneling. From the overall spread of the spectrum and the low intensity of the extra tunneling peaks, we may conclude that the tunneling frequency in TCTMB- d_3 is higher than the deuterium quadrupole interaction, indicating that the CD_3 groups can rotate fairly unhindered.¹⁹

5 Summary and conclusions

This work demonstrates the power of deuterium single crystal NMR spectroscopy as a complementary tool for X-ray crystallography. We have applied this method to quantitatively study the population distribution (otherwise referred to as orientational disorder) and the jump rates between different orientations in the solid phases of TCTMB. The high temperature monoclinic phase was found by an earlier X-ray investigation⁴ to be orientationally disordered, which was ascribed to the pseudo-hexagonal symmetry of the TCTMB molecules. The NMR method is extremely sensitive to the population distribution between different orientations and in the present study we found a considerable deviation from equal distribution (planar disorder). On cooling within the monoclinic phase, the population distribution becomes more polarized, as if the system senses the low temperature triclinic phase, which from the low temperature X-ray measurements of Fourme and Renaud⁵ at 173 K, is expected to be highly ordered. It is interesting that these authors realized, mainly on

the basis of the observed temperature factors, that the ordering at this temperature is not complete, and concluded that the molecules are probably not fully polarized above 100 K. Our deuterium NMR results are consistent with this view and indicate that the disorder increases continuously on heating towards the monoclinic phase. Thus, the transformation from a perfectly ordered triclinic phase to a disordered monoclinic phase is a very gradual process, spanning a wide temperature range. The actual transition takes place between two partially ordered phases, and is consequently only weakly first order. It does not involve any major structural changes of the lattice but merely a relatively small, discontinuous change in the molecular polarization.

The phenomenon of transition between partially ordered phases probably also occurs in other mixed chloromethylbenzenes. Clearly, the packing potential of these molecules is not perfectly hexagonal and depends not only on the shape of the isolated molecule, but to a large extent also on the arrangement of the neighboring molecules in the lattice. Consequently a wide range of order/disorder can be expected in the solid phases of the $C_6Cl_n(CH_3)_{6-n}$ compounds, from perfect order to perfect disorder. The present system, at high temperatures, is close to the latter situation. It is remarkable, however, that already sixty years ago,¹ it was suggested that the disorder in TCTMB is not complete, in order to account for anomalous dielectric relaxation effects observed in this compound. An example of a highly ordered chloromethylbenzene is the isomeric compound, 1,3,5-trichloro-2,4,6-trimethyl benzene, where X-ray measurements² indicate that, although the molecules undergo rapid in-plane reorientation, they exhibit complete orientational order. Thus, in this case, the packing energy of the lattice well discriminates between chlorine and methyl substituents.

Another virtue of the NMR method is its usefulness in the study of molecular rate processes over extremely wide dynamic ranges. The pretransition region in both the monoclinic phase on cooling and in the triclinic phase on heating extends over a very wide temperature interval, over which there is a monotonic increase in the rate of the molecular reorientation, from about 10^3 s^{-1} at 180 K to 10^{13} s^{-1} at 400 K.

Finally, we mention the ability of the single crystal deuterium NMR method to characterize the dynamics of the methyl group. For TCTMB, above 15 K, the dominating process is the thermally activated reorientation, which we studied by T_1 relaxation. Below 15 K, this incoherent

(classical) process is replaced by quantum mechanical coherent tunneling. Although we have not quantitatively studied this regime in the present work, we could demonstrate the presence of tunneling by identifying its characteristic features in the deuterium NMR spectrum.

Acknowledgement

This work was supported by the German-Israeli Foundation, G.I.F. Project No. I-558.218.05/97 and by the G.M.J. Schmidt Minerva Center for Supramolecular Architecture.

References

- 1 A. H. White, B. S. Biggs and S. O. Morgan, *J. Am. Chem. Soc.*, 1940, **62**, 16.
- 2 M. Tazi, J. Meinel, M. Sanquer, M. Nusimovici, F. Tonnard and R. Carrie, *Acta Crystallogr. Sect. B*, 1995, **51**, 838.
- 3 C. Brot and I. Darmon, *J. Chem. Phys.*, 1970, **53**, 2271.
- 4 R. Fourme, M. Renaud and D. Andre, *Mol. Cryst. Liq. Cryst.*, 1972, **17**, 209.
- 5 R. Fourme and M. Renaud, *Mol. Cryst. Liq. Cryst.*, 1972, **17**, 223.
- 6 C. Brot, I. Darmon and N. Dat-Xuong, *J. Chim. Phys.*, 1967, **64**, 1061.
- 7 J.-M. Chezeau, J. H. Strange and C. Brot, *J. Chem. Phys.*, 1972, **56**, 1380.
- 8 T. Bräuniger, R. Poupko, Z. Luz, P. Gutsche, C. Meinel, H. Zimmermann and U. Haeberlen, *J. Chem. Phys.*, 2000, **112**, 10858.
- 9 Actually, the existence of two domain types with a statistical (equal) distribution in the triclinic phase was inferred by Fourme and Renaud from the overall monoclinic symmetry (with doubling of the b and c repeats) of the 173 K diffraction pattern. The α and β domains are, in fact, derivative structures of the monoclinic space group $P2_1/c$. A general discussion of "derivative structures" in terms of space group hierarchies has been given by M. J. Buerger, *J. Chem. Phys.*, 1947, **15**, 1.
- 10 J. Hirschinger and A. D. English, *J. Magn. Reson.*, 1989, **85**, 542.
- 11 D. Reichert and H. Schneider, *Z. Phys. Chem.*, 1995, **190**, 63.
- 12 C. Schmidt, B. Blümich and H. W. Spiess, *J. Magn. Reson.*, 1988, **79**, 269.
- 13 A. Heuer, *J. Magn. Reson.*, 1990, **89**, 287.
- 14 W. Schajor, PhD Thesis, University of Heidelberg, 1983.
- 15 B. Tesche, H. Zimmermann, R. Poupko and U. Haeberlen, *J. Magn. Reson. A*, 1993, **104**, 68.
- 16 K. Schmidt-Rohr and H. W. Spiess, *Multidimensional Solid-State NMR and Polymers*, Academic Press, London, 1994, pp. 444–448.
- 17 D. A. Torchia and A. Szabo, *J. Magn. Reson.*, 1982, **49**, 107.
- 18 A. Detken, P. Focke, H. Zimmermann, U. Haeberlen, Z. Olejniczak and Z. T. Lalowicz, *Z. Naturforsch. A*, 1995, **50**, 95.
- 19 M. Prager and A. Heidemann, *Chem. Rev.*, 1997, **97**, 2933.